Nuclear Lamin A/C Deficiency Induces Defects in Cell Mechanics, Polarization, and Migration

Jerry S. H. Lee,* Christopher M. Hale,* Porntula Panorchan,* Shyam B. Khatau,* Jerry P. George,* Yiider Tseng,¶ Colin L. Stewart,† Didier Hodzic,§ and Denis Wirtz*‡

*Department of Chemical and Biomolecular Engineering, and ‡Institute for NanoBioTechnology and Howard Hughes Medical Institute graduate training program, Johns Hopkins University, Baltimore, Maryland; †Cancer and Developmental Biology, National Cancer Institute, Frederick, Maryland; §Department of Cell Biology and Physiology, Washington University School of Medicine, St. Louis, Missouri; and ¶Department of Chemical Engineering, University of Florida, Gainesville, Florida

ABSTRACT Lamin A/C is a major constituent of the nuclear lamina, a thin filamentous protein layer that lies beneath the nuclear envelope. Here we show that lamin A/C deficiency in mouse embryonic fibroblasts ($Lmna^{-/-}$ MEFs) diminishes the ability of these cells to polarize at the edge of a wound and significantly reduces cell migration speed into the wound. Moreover, lamin A/C deficiency induces significant separation of the microtubule organizing center (MTOC) from the nuclear envelope. Investigations using ballistic intracellular nanorheology reveal that lamin A/C deficiency also dramatically affects the micromechanical properties of the cytoplasm. Both the elasticity (stretchiness) and the viscosity (propensity of a material to flow) of the cytoplasm in $Lmna^{-/-}$ MEFs are significantly reduced. Disassembly of either the actin filament or microtubule networks in $Lmna^{+/+}$ MEFs results in decrease of cytoplasmic elasticity and viscosity down to levels found in $Lmna^{-/-}$ MEFs. Together these results show that both the mechanical properties of the cytoskeleton and cytoskeleton-based processes, including cell motility, coupled MTOC and nucleus dynamics, and cell polarization, depend critically on the integrity of the nuclear lamina, which suggest the existence of a functional mechanical connection between the nucleus and the cytoskeleton. These results also suggest that cell polarization during cell migration requires tight mechanical coupling between MTOC and nucleus, which is mediated by lamin A/C.

INTRODUCTION

The nuclear envelope (NE) is composed of two lipid bilayers, the inner and the outer nuclear membrane (INM and ONM, respectively). The ONM, an extension of the rough endoplasmic reticulum (ER), is connected to the INM at the nuclear pore complex. The INM and the ONM delineate the periplasmic space, which is continuous with the ER lumen (1). INM proteins interact directly with the nuclear lamina, a specialized meshwork of lamins that constitute the type V intermediate filament family. In mammals, the alternative splicing of a single gene encodes A-type lamins (lamin A, AΔ10, C2), while B-type lamins (B1, B2, B3) are encoded by two distinct genes (2,3). Besides exhibiting the general organization of an intermediate filament—a central rod domain composed of four coiled-coil domains flanked by an N-terminal globular head and a C-terminal tail—lamins possess a nuclear localization signal as well as a farnesylation site in the C-terminal tail of most isoforms. While A-type lamins are developmentally regulated, B-type lamins are essential for viability (4,5).

Scattered mutations in the lamin A/C gene (*Lmna*) are responsible for a broad range of human diseases termed laminopathies (6,7). These include Emery-Dreifuss muscular dystrophy (EDMD) (8), dilated cardiomyopathy (9), Dunnigan-type partial lipodystrophy (10), limb girdle muscular dystrophy 1B (11), Charcot-Marie-tooth syndrome type 2B1 (12), mandibuloacral dysplasia (MAD) (13), the Hutchinson-Gilford progeria (HGPS) (14,15), and some atypical progeroid syndromes (16). Phenotypical manifestations of these diseases consist of either specific or combined pathologies of skeletal and cardiac muscle, neurons, bone, and adipose tissues (14). To date, nearly 200 mutations have been described in ~900 patients; except for some mutational ''hot spots'' in FPLD, MAD, and HGPS (17), the position of pathological mutation of *Lmna* is not predictive of the disease phenotype.

Mouse models either lacking lamin A/C or expressing mutated versions display phenotypes that mimic the human pathologies associated with the corresponding mutations. Mice lacking lamin A/C (18) develop cardiac and skeletal myopathies reminiscent of human EDMD. Knock-in mice expressing mutant $Lmna^{L530P/L530P}$ (19), $Lmna^{N195K/N195K}$ (20), or $Lmna^{H222P/H222P}$ (21) display phenotypes similar to human HGPS, dilated cardiomyopathy, and striated muscle laminopathies, respectively.

The pathophysiological mechanisms of *Lmna* mutations are still unknown. However, these mutations are thought to cause defects in gene regulation and/or in mechanical properties of affected cells. The gene regulation hypothesis is based on the association of lamin A/C with chromatin and several

Submitted January 15, 2007, and accepted for publication May 11, 2007.

Jerry S. H. Lee, Christopher M. Hale, and Porntula Panorchan contributed equally to this work.

Address reprint requests to Didier Hodzic, Dept. of Cell Biology and Physiology, Washington University School of Medicine, 660 S. Euclid Ave., St. Louis, MO 63110. Tel: 314-362-1082; or to Denis Wirtz, Dept. of Chemical and Biomolecular Engineering, Johns Hopkins University, 3400 N. Charles St., Baltimore, MD 21218. Tel: 410-516-7006; Fax: 410-516-5510.

Editor: Michael Edidin.

0006-3495/07/10/2542/11 $2.00

doi: 10.1529/biophysj.106.102426

proteins involved in gene regulation (22) and the direct involvement of lamins in transcription (23). Gene expression deregulation is further exemplified by an early hyperproliferation followed by increased rate of apoptosis of aging HGPS cell culture (24). A mechanical hypothesis for disease etiology is based on the observation that cells harboring *Lmna* mutations often display ultrastructural anomalies of their nuclei as well as the loss of NE localization of structural proteins. Furthermore, mouse embryonic fibroblasts lacking lamin A/C display a ''fragile nucleus'' (25) and an apparent loss of cytoplasmic mechanical stiffness (26).

The hard-wiring of the nucleus to the cytoskeleton has been directly demonstrated (27). In addition, in mouse cardiomyocytes, the lack of lamin A/C induces the disorganization of the sarcoplasmic desmin network (28) and our recent results demonstrate that the lack of lamin A/C disrupts a macromolecular complex that spans the nuclear envelope and physically connects the nucleoskeleton to the cytoskeleton (29). We therefore hypothesize that, in addition to NE structural defects, mutations of lamin A/C induce cytoskeletal defects. In this study, the recently introduced method of ballistic intracellular nanorheology (BIN) (30,31) is used to compare the cytoplasmic plasticity of mouse embryonic fibroblasts lacking lamin A/C ($Lmna^{-/-}$ MEFs) with their wild-type (WT) littermates ($Lmna^{+/+}$ MEFs). BIN assay measures directly and rigorously the mechanical properties of the cytoskeleton, not the composite response of the cytoplasm, the plasma membrane, and the nucleus, as measured previously (26). We then investigated whether lamin A/C deficiency affects cytoskeleton-mediated processes, including MTOC positioning with respect to the nucleus, cell polarization, and cell migration.

MATERIALS AND METHODS

Cell culture

$Lmna^{+/+}$ and $Lmna^{-/-}$ MEFs were cultured in DMEM-high glucose (HyClone, Logan, UT) supplemented with 10% bovine growth serum (HyClone) and 100 units of penicillin/100 μg of streptomycin (Sigma, St. Louis, MO) and maintained at 37°C in a humidified, 5% CO_2 environment. Cells (initial passage 22) were passaged every 2–3 days for a maximum of six passages. For wounding, the cells were seeded ($\sim 6.3 \times 10^3$ cell/ml) onto 35-mm glass bottom dishes (MaTek, Ashland, MA). For ballistic nanoparticle injection (see below), cells were seeded ($\sim 1 \times 10^4$ cell/ml) on 10-cm cell culture dishes (Corning, Corning, NY).

Cell migration

MEFs plated on 35-mm glass bottom dishes were cultured to a confluent monolayer and scratched using a 20 gauge, 1.5-in hypodermic needle (Becton, Dickinson & Co., Franklin Lakes, NJ). When indicated, cells were treated with nocodazole or latrunculin B (as described below). Control and drug-treated cells were rinsed of detached cells and phase contrast images were collected every hour using a Cascade 1K CCD camera (Roper Scientific, Tucson, AZ) mounted on a Nikon TE2000E microscope with a 10× Plan Fluor lens (N.A. 0.3, Nikon, Melville, NY) controlled by Metavue software (Universal Imaging, West Chester, PA). Image analysis was conducted by tracing the edge of the wound and calculating the remaining wound area using Metamorph software (Universal Imaging). Wound areas of comparable sizes were used to avoid variability of closure time.

Cell polarization

Polarization was assessed based on the location of the microtubule organizing center (MTOC) relative to the wound. A cell was deemed polarized if its MTOC was located in the radial third of the cell facing the wound. Cells were fixed at 1-h intervals postwound (0–3 h) and stained for nuclear DNA and microtubules. Cells were fixed with 2% paraformaldehyde for 1 h. Cells were then permeabilized with 0.1% Triton X-100 for 10 min. Bovine calf serum (BCS) (10%) in phosphate-buffered saline was used to block nonspecific binding for 20 min and the cells were then incubated with an α-tubulin monoclonal antibody (Oncogene, Boston, MA) at 1:20 dilution. Next, cells were incubated in Alexa-568 goat anti-mouse antibody at 1:40 and 300 nM DAPI for 1 h (Invitrogen, Carlsbad, CA) to visualize microtubules and nuclear DNA, respectively. MTOC location was determined by overlaying Alexa-568 and DAPI fluorescence images using Metamorph. Fluorescent images were taken using a Cascade 1 K charge-coupled device (CCD) camera (Roper Scientific) mounted on a Nikon TE2000E microscope with a 60× Plan Fluor lens (N.A. 1.4, Nikon) controlled by the software Metavue.

MTOC positioning

MEFs plated on 35-mm glass bottom dishes were fixed, permeabilized, and blocked as described above. Cells were then stained for nuclear DNA and γ-tubulin. Following BCS incubation, cells were incubated with a γ-tubulin rabbit polyclonal antibody (Abcam, Cambridge, MA) at 1:500 dilution. Next, cells were incubated in Alexa-568 goat anti-rabbit antibody at 1:40 and 300 mM DAPI for 1 h (Invitrogen) to visualize the MTOC and nuclear DNA, respectively. MTOC position relative to nucleus was determined by overlaying Alexa-568 and DAPI fluorescence images using Metamorph. Fluorescent images were taken as described above. A value of 0 was assigned to a cell if the MTOC touched or laid on top or bottom of the nucleus, whereas a value of 1 was assigned to a cell if the MTOC was clearly separated from the nucleus.

Drug treatments

The microtubule-destabilization drug nocodazole (Sigma) and the F-actin disassembly drug latrunculin B (Sigma) were diluted from the stock DMEM-high media (described above). Nocodazole was used at a final concentration of 1 μg/ml. Latrunculin B was used at a final concentration of 5 μg/ml. Cells were incubated with either nocodazole or Latrunculin B for 30 min before wounding. Drug concentrations were maintained during experiments to avoid recovery.

Ballistic intracellular nanorheology

The recently introduced method of ballistic intracellular nanorheology (BIN) (30,31) was used to measure rigorously the mechanical properties of the cytoplasm of MEFs. Fibroblasts plated on 10-cm cell culture dishes were subjected to ballistic injection of 100-nm diameter fluorescent polystyrene nanoparticles (Invitrogen) using a Biolistic PDS-1000/HE particle delivery system (Bio-Rad, Richmond, CA). Nanoparticles were coated on macrocarriers and allowed to dry for 2 h. Rupture disks (2200 psi) were used in conjunction with a hepta-adaptor. Problems could arise when nanoparticles do not penetrate directly the cytoplasm upon impact, which may then be engulfed by the cell through endocytosis and then undergo microtubule-mediated directed motion (32). We circumvented this problem by thoroughly and repeatedly washing the cells with fresh medium right after ballistic bombardment. We found that none of the probed nanoparticles underwent directed motion.

A region of interest (ROI) was generated using Metavue software for recording particle videos. The ROI was optimized so that a 3 × 3 binning acquisition using the Cascade 1K CCD camera yielded movies that were 30 frames per second. Using a 60× Plan Fluor oil-immersion lens (N.A. 1.4, Nikon), movies capturing the Brownian motion of the injected nanoparticles were collected and analyzed first using Metamorph software (Universal Imaging). Subsequent use of a second custom software was used to obtain rheological parameters describing the viscoelastic properties of the cytoplasm (33), including elastic and viscous moduli, shear viscosity, and creep compliance. At least 200 different nanoparticles were tracked per condition.

The time-averaged mean squared displacement (MSD), $\langle \Delta r^2(\tau) \rangle = \langle [x(t+\tau) - x(t)]^2 + [y(t+\tau) - y(t)]^2 \rangle$, where τ is the timescale and t is the elapsed time, was calculated from the trajectory of the light intensity-weighted centroid of each nanoparticle. Previous studies have examined the effects of size and surface chemistry of the nanoparticles in cells (32,34). It is important to note that each movie is much shorter than that the characteristic timescales of cell migration. We assumed that the time-averaged movements of the nanoparticles in the x-, y-, and z-directions were identical. To test this assumption, we verified and found that the MSDs of individual nanoparticles in the x- and y-directions were identical, $\langle \Delta x^2(\tau) \rangle = \langle \Delta y^2(\tau) \rangle$ so that $\langle \Delta r^2(\tau) \rangle = 2\langle \Delta x^2(\tau) \rangle = 2\langle \Delta y^2(\tau) \rangle$ (35). This suggests that, for the short times of movie capture, the cytoplasm around each nanoparticle can be considered to be isotropic, i.e., it has the same physical properties in the x- and y-directions, and therefore the z-direction.

By tracking the centroid displacements of the nanoparticles, we can reach subpixel spatial resolution of 10 nm. A small displacement of the nanoparticle will induce a displacement of the centroid of the light-intensity profile of the diffraction-limited image of each nanoparticle, which is readily detected with subpixel resolution. We measured directly the displacement resolution of our tracking method by tethering the same type of nanoparticles that we used in the live-cell experiments to a glass coverslip and probed the apparent displacements of those nanoparticles. The square root of the MSDs of these ''immobile'' nanoparticles is the real displacement resolution of our microscopy/particle-tracking system, which we find to be ~10 nm.

The MSD of each probe nanoparticle is directly related to the local creep compliance of the cytoplasm, $\Gamma(\tau)$, as (36)

$$\Gamma(\tau) = \frac{3\pi a}{2k_B T} \langle \Delta r^2(\tau) \rangle.$$

The creep compliance (expressed in units of cm^2/dyn, the inverse of pressure or modulus) describes the local deformation of the cytoplasm induced by the small random forces acting on the surface of the nanoparticles and created by the thermally excited displacements of the nanoparticles. The local frequency-dependent viscoelastic parameters of the cytoplasm, $G'(\omega)$ and $G''(\omega)$ (both expressed in units of dyn/cm^2, a force per unit area), are computed straightforwardly from the MSD (see the literature (32,34) for details). The elastic modulus, G', and viscous modulus, G'', describe the propensity of a complex fluid to store energy and to flow under mechanical stress, respectively. A cross-linked filamentous structure, such as a reconstituted F-actin network (37) or the cytoplasm (38), behaves like a solid elastic gel at high rates of shear (high frequencies ω), because the filaments do not have the time to relax during shear, and like a liquid at low rates of shear. The crossover rate of shear at which these two rheological behaviors are identical (the frequency at which $G'(\omega) = G''(\omega)$) corresponds to the inverse of the relaxation time. The mean shear viscosity of the cytoplasm can be approximated as the product of the mean relaxation time and the mean plateau value of the elastic modulus of the cytoplasm. Here we report the shear viscosity and the plateau modulus of the cytoplasm of MEFs.

Statistical analysis

Mean values, standard error of measurement (mean ±SE), and statistical analysis for creep compliance, elastic modulus, and shear viscosity were calculated using Graphpad Prism (Graphpad Software, San Diego, CA) and plotted using Kaleidagraph (Reading, PA) for these rheological parameters. Two-tailed unpaired t-tests were conducted within control and drug-treated conditions to determine the significance of change caused by shear stimuli. Significant difference is indicated in the figures using the standard Michelin Guide scale: *** for $p < 0.001$, ** for $p < 0.01$, and * for $p < 0.05$. One-way ANOVA tests were also conducted across conditions for elastic moduli and shear viscosity values, and corresponding P-values are reported.

RESULTS

Lamin A/C deficiency mechanically weakens the cytoplasm of MEFs

We assessed quantitatively the effect of lamin A/C deficiency on the mechanical behavior of the cytoplasm of MEFs using the recently introduced method of ballistic intracellular nanorheology (30). Unlike other conventional methods that measure cell mechanics from the outside of the cell (see more under Discussion), BIN probes directly the cytoplasm of live cells. Fluorescent nanoparticles (100-nm diameter) were ballistically bombarded in the cytoplasm of adherent MEFs. After 12-h incubation, the nanoparticles (*yellow beads*, Fig. 1) had dispersed evenly within the cytoplasm. These nanoparticles were subsequently tracked with high spatial and temporal resolutions using time-lapsed fluorescence microscopy (Fig. 1, *A* and *B*). The same nanoparticles have been shown not to interfere with basic cell functions and not to interact with subcellular structures (32). Ballistic injection of the probe nanoparticles allowed us to probe a large number of individual cells and, like manual microinjection, circumvented the endocytosis of the nanoparticles and, therefore, eliminated their eventual directed motion in the cytoplasm. The random Brownian displacements of the nanoparticles in the cytoplasm were analyzed to rigorously infer the local viscoelastic properties of the cytoplasmic milieu.

The movements of the centroids of the nanoparticles in at least 20 cells were monitored for 20-s time spans, for a total of at least 200 different nanoparticles for each tested condition. A time of 20 s is orders-of-magnitude shorter than the timescales controlling the slow locomotion of MEFs. The magnitude and time lag-dependence of the mean squared displacement (MSD) of each nanoparticle (Fig. 1 *C*) directly reflects and quantifies the viscoelastic character of the cytoplasm in the vicinity of that nanoparticle. If the MSD of a nanoparticle grows linearly with time lag, $\langle \Delta r^2(\tau) \rangle \sim \tau$ (the symbol $\sim$ signifies ''is proportional to''), then it moves by random diffusion in a simple viscous liquid. If its MSD grows more slowly than the time lag, $\langle \Delta r^2(\tau) \rangle \sim \tau^\alpha$ with $\alpha < 1$, then that nanoparticle moves in a milieu that is both viscous and elastic. If the MSD grows more rapidly than time, $\langle \Delta r^2(\tau) \rangle \sim \tau^\alpha$ with $\alpha > 1$, then the nanoparticle undergoes convective or directed transport, which was never observed in our experiments (Fig. 1 *C*). Therefore, the slope of the MSD, α, describes whether the cytoplasm has a viscous character like a liquid or an elastic character like a solid or is both viscous and elastic (i.e., viscoelastic). The extent of the

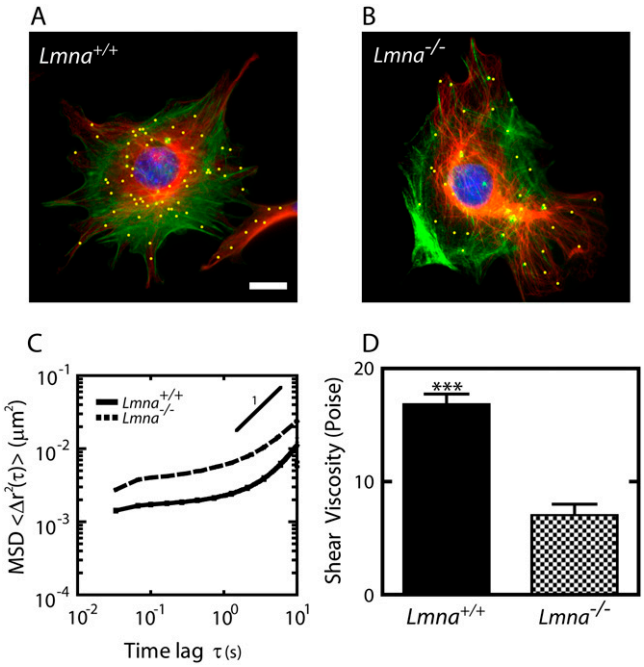

FIGURE 1 Altered mechanical properties of the cytoplasm in MEFs lacking lamin A/C. (*A* and *B*) Immunofluorescence micrographs of the actin filament (*green*) and microtubule (*red*) networks in $Lmna^{+/+}$ MEFs (*A*) and $Lmna^{-/-}$ MEFs (*B*), overlaid with fluorescence micrographs of ballistically injected 100-nm diameter nanoparticles (*yellow*). Cells were fixed and actin, microtubule, and nuclear DNA were stained using Alexa-488 phallodin, α-tubulin/Alexa568, and DAPI, respectively. Nanoparticles were enlarged for ease of visualization. Bar, 20 μm. (*C*) Average mean-squared displacements (*MSD*) of nanoparticles imbedded in the cytoplasm of $Lmna^{+/+}$ MEFs (*solid line*) and $Lmna^{-/-}$ MEFs (*dashed line*) ($n > 35$ cells each). A higher value of MSD indicates larger movements of the particles, which indicates a softer cytoplasm. (*D*) Average shear viscosity of the cytoplasm of $Lmna^{+/+}$ MEFs (*left*) and $Lmna^{-/-}$ MEFs (*right*) calculated from the MSDs ($n > 35$ cells each).

displacements quantifies the levels of viscosity and elasticity of the cytoplasm.

The MSDs of nanoparticles embedded in the cytoplasm of MEFs showed some variations, but all exhibited subdiffusive motion over a narrow range of displacements (Fig. 1 *C*). Indeed, a log-log plot of the MSD as a function of time indicated that the MSD displayed a slope smaller than 1, but larger than zero. Therefore, the cytoplasm of MEFs is viscoelastic. As described previously (32), a simple mathematical manipulation transforms MSDs into rheological parameters that rigorously describe the deformability and the viscoelastic properties of the cytoplasm, including shear viscosity (Fig. 1 *D*), elasticity (Fig. 2 *B*), and creep compliance (Fig. 2 *C*). Here we report all three parameters because different rheological assays report different parameters. The cytoplasm of $Lmna^{-/-}$ MEFs was significantly more compliant (i.e., more deformable) (Fig. 2 *D*), less elastic (Fig. 2 *B*), and less viscous (Fig. 1 *D*) than the cytoplasm of $Lmna^{+/+}$ MEFs. In particular, the elasticity of the cytoplasm was 50% lower in cells lacking lamin A/C than in WT cells. The shear viscosity of the cytoplasm was also ~50% lower. Together these results indicate that the cytoplasm of MEFs lacking lamin A/C is significantly softer and less viscous than the cytoplasm of control MEFs.

Difference in stiffness between perinuclear region and lamella is regulated by lamin A/C

BIN combined with phase contrast microscopy allowed us to probe the mechanical properties of different regions of the cytoplasm in living cells. We have shown previously that the actin-rich cell periphery is significantly stiffer than the perinuclear region in adherent cells (32,34). We hypothesized that if a mechanical link between nucleus and cytoskeleton existed then lamin A/C deficiency would reduce the differences in stiffness between regions inside and outside the perinuclear region. To test this hypothesis, we measured the mechanical properties inside and outside a 30-μm diameter circular region centered on the nucleus (Fig. 3, *A* and *B*). This circle approximately delineates the perinuclear region from the rest of the body of the cell, which we denominate as the lamella. In $Lmna^{+/+}$ MEFs, we found that the deformability of the cytoplasmic region around the nucleus was significantly higher than the rest of the cytoplasm (Fig. 3 *C*). Moreover, in $Lmna^{+/+}$ MEFs, the shear viscosity of the perinuclear region was significantly lower than the shear viscosity of the lamella (Fig. 3 *D*). The difference in deformability and viscosity between cytoplasmic regions inside and outside the perinuclear region was much smaller in $Lmna^{-/-}$ MEFs (Fig. 3, *C* and *D*). Therefore lamin A/C deficiency diminishes greatly the difference in the mechanical properties between lamella and perinuclear region.

Regulation of cytoskeleton plasticity by lamin A/C

Next, we determined how actin and microtubule networks contributed to the cytoplasmic viscoelasticity of $Lmna^{+/+}$ and $Lmna^{-/-}$ MEFs. Treatment of MEFs with latrunculin B depolymerized actin without affecting significantly microtubule organization (Fig. 2 *A*). Latrunculin B treatment decreased significantly the stiffness and increased the mechanical deformability of the cytoplasm of $Lmna^{+/+}$ MEFs, but had no significant effect on the stiffness and deformability of $Lmna^{-/-}$ MEFs (Fig. 2, *B–D*). Treatment of MEFs with nocadozole disassembled the microtubule network, without affecting significantly the architecture of the actin cytoskeleton (Fig. 2 *A*). Nocadozole treatment decreased significantly the stiffness and mechanical compliance of the cytoplasm of WT cells, but had no significant effect on the mechanical properties of the lamin A/C knockout cells (Fig. 2, *B–D*). Since the disassembly of either the actin network or the microtubule network did not affect intracellular micromechanical properties of knockout MEFs, these results indicate that the mechanical deformability of the cytoskeleton in

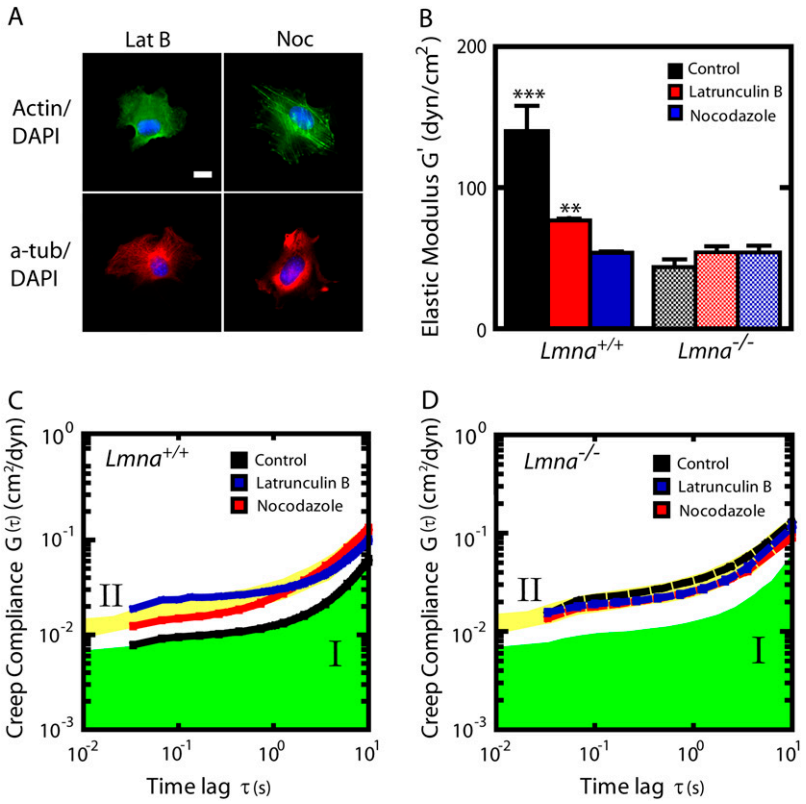

FIGURE 2 Mechanical behavior of $Lmna^{+/+}$ and $Lmna^{-/-}$ MEFs following actin filament or microtubule disassembly. (*A*) Immunofluorescence micrographs of the actin (*green*) and microtubule (*red*) networks in $Lmna^{+/+}$ and $Lmna^{-/-}$ cells treated with either latrunculin B or nocadozole. Cells were fixed and actin, microtubule, and nuclear DNA were stained using Alexa-488 phallodin, α-tubulin/Alexa568, and DAPI, respectively. Bar, 20 μm. (*B*) Average elasticity of the cytoplasm of control and drug-treated $Lmna^{+/+}$ (*left columns*) and $Lmna^{-/-}$ (*right columns*) MEFs ($n > 25$ cells were assayed for each condition). (*C* and *D*) Average creep compliance of the cytoplasm of control and drug-treated $Lmna^{+/+}$ MEFs (*C*) and $Lmna^{-/-}$ MEFs (*D*). At least 25 cells were assayed for each condition. For ease of comparison, the green area indicates the compliance of control cells (regime *I*) and the yellow area indicates the compliance of the knockout cells (regime *II*).

MEFs depends critically on the integrity of the nuclear lamina.

Lamin A/C deficiency reduces the speed of cell migration and abrogates MTOC polarization

Our previous work has shown that fibroblasts stiffen their cytoplasm when they migrate into a wound (34). Since lamin A/C deficiency alters intracellular mechanics, we hypothesized that the softening of the cytoskeleton on lamin A/C deficient cells would impact cytoskeleton-based cellular processes such as directed cell migration and polarization.

To investigate the effect of lamin A/C deficiency on cell migration, $Lmna^{+/+}$ and $Lmna^{-/-}$ MEFs were grown to a confluent monolayer, and subsequently scratched to create a ~200-μm wide wound. The rate of wound healing was monitored and quantified over 3 h (Fig. 4). The results showed that wound closure occurred significantly faster in $Lmna^{+/+}$ MEFs than in $Lmna^{-/-}$ MEFs (Fig. 4 *B*). Depolymerization of either F-actin or microtubules by drug treatments greatly reduced the speed of wound healing of $Lmna^{+/+}$ MEFs, but had little added effect on the (already slow) speed of wound healing of $Lmna^{-/-}$ MEFs (data not shown).

In addition to measuring rates of wound closure, we also examined changes in polarity, determined by the location of the MTOC with respect to the wound edge. It is well-established that cells at the edge of a wound tend to exhibit a polarized microtubule network (39–41). If cells at the edge are split into thirds, the MTOC (or centrosome) is typically found in the third facing the wound (Fig. 5 *B*). We found that $Lmna^{+/+}$ MEFs progressively repositioned their MTOC preferentially in the direction of the wound over 3 h (Fig. 5 *C*, *black bars*). This preferential localization of the MTOC toward the wound was not observed in $Lmna^{-/-}$ MEFs (Fig. 5 *C*, *checkered bars*). Together these results suggest that the absence of nuclear lamin A/C not only significantly reduces the speed of wound closure migration, but also largely eliminates wound-induced cell polarization.

Lamin A/C deficiency separates the MTOC from the nuclear envelope

The previous measurements suggest the existence of a mechanical connection between the nuclear envelope and the MTOC. To further test this hypothesis, we used immunofluorescence microscopy to measure the apparent distance between the MTOC, marked by γ-tubulin staining, and the nuclear envelope of $Lmna^{+/+}$ MEFs and $Lmna^{-/-}$ MEFs, marked by DAPI staining. In control $Lmna^{+/+}$ MEFs, the MTOC was found either right next to the nuclear envelope or located under or above the nucleus. By contrast, lamin A/C deficiency created significant separation between MTOC and nuclear envelope (Fig. 6). The apparent distance between

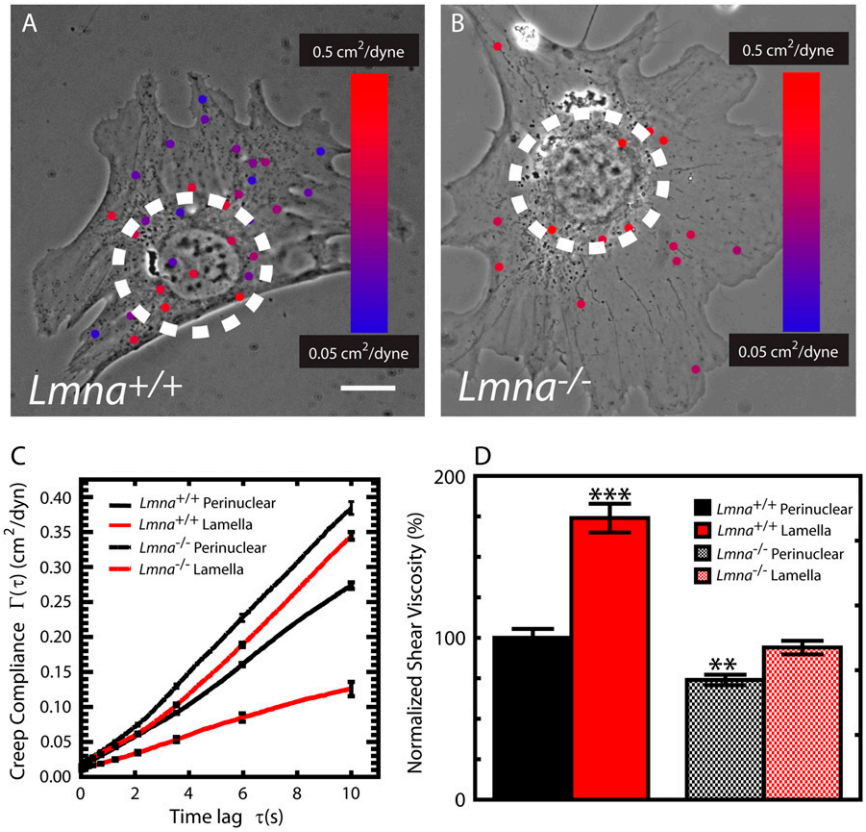

FIGURE 3 Effect of lamin A/C deficiency on the mechanical properties of the perinuclear region and the lamella. (*A* and *B*) ''Heat'' maps of the local mechanical properties of MEFs. Phase contrast micrographs of $Lmna^{+/+}$ MEF (*A*) and $Lmna^{-/-}$ MEFs (*B*) superimposed with fluorescence micrographs of the probe nanoparticles embedded in their cytoplasm. The circles are 30 μm in diameter and centered on the nuclei centers; they delineate the perinuclear region from the lamella. Nanoparticles are color-coded according to the local compliance of the cytoplasm in the vicinity of each nanoparticle. Blue corresponds to stiff regions and red to soft regions of the cell. The size of the nanoparticles is augmented for ease of view. Bar, 10 μm. (*C*) Average creep compliance of the perinuclear region and lamella of $Lmna^{+/+}$ MEFs and $Lmna^{-/-}$ MEFs. At least 25 cells were assayed for type of cell. Linear scales are used for compliance and time lag to highlight differences. (*D*) Average shear viscosity in the perinuclear region and the lamella of $Lmna^{+/+}$ MEFs and $Lmna^{-/-}$ MEFs. Shear viscosity values were normalized with the shear viscosity of the perinuclear region of $Lmna^{+/+}$ MEFs. At least 25 cells were assayed for each type of cell.

MTOC and nucleus could be as high as 5.80 μm in $Lmna^{-/-}$ MEFs; the mean MTOC-nucleus distance was 1.5 μm. In control cells, the MTOC-nucleus distance never exceeded 0.8 μm. This result suggests that lamin A/C mediates a tight mechanical connection between the MTOC and the nucleus.

DISCUSSION

A mechanical link between cytoskeleton and nucleus mediated by lamin A/C

Recent studies have provided compelling evidence for the existence of physical connections between the nucleoplasm and the cytoskeleton. In live endothelial cells, micromanipulation suggested the existence of such a physical connection (27). Furthermore, nuclear shape can be drastically altered by the depolymerization of actin and/or microtubule networks in several cell types (42,43) and suggests a physical connection of these networks to the nucleus. MTOC positioning and nucleus positioning are controlled by the same signaling pathways in fibroblasts under shear forces (42). The molecular nature of two such connections has been unraveled in *Caenorhabditis elegans*: ZYG-12 has been shown to mediate the essential attachment of the centrosome to the nucleus (44) and Ce-lamin with UNC-84 and ANC-1 are involved in actin-dependent anchorage of the nucleus (45–48). Recent studies suggest that the latter anchoring mechanism is evolutionary-conserved in mammalian cells (29).

Therefore, we used $Lmna^{-/-}$ MEFs to investigate whether cell functions that could depend on these links were affected in comparison to $Lmna^{+/+}$ MEFs. BIN studies show that the absence of nuclear lamin A/C increases dramatically the deformability of the cytoplasm of $Lmna^{-/-}$ MEFs. The elasticity, which describes the stretchiness of the cytoplasm, and the viscosity, which describes its propensity to flow like a liquid, in $Lmna^{-/-}$ MEFs are both reduced approximately by 50%. Importantly, the extent of $Lmna^{-/-}$ MEF softening is as significant as that observed in WT MEFs treated with actin-disassembly or microtubule-disassembly agents. Moreover, the depletion of lamin A/C largely homogenizes the stiffness throughout the cytoplasm, eliminating the sharp difference in the mechanical properties between the perinuclear region and the lamella observed in WT cells. These results suggest the new and important conclusion that global cytoskeleton mechanics depend crucially on the molecular links between the actin and microtubule cytoskeletons and the nuclear lamina.

A toy model of how cytoplasmic mechanics could be enhanced by the nucleus/cytoskeleton link can be described as follows. Let us imagine a rubber ball (i.e., the nucleus) inside a bag full of rubber bands and liquid (i.e., the viscoelastic cytoplasm). When the ball is not physically

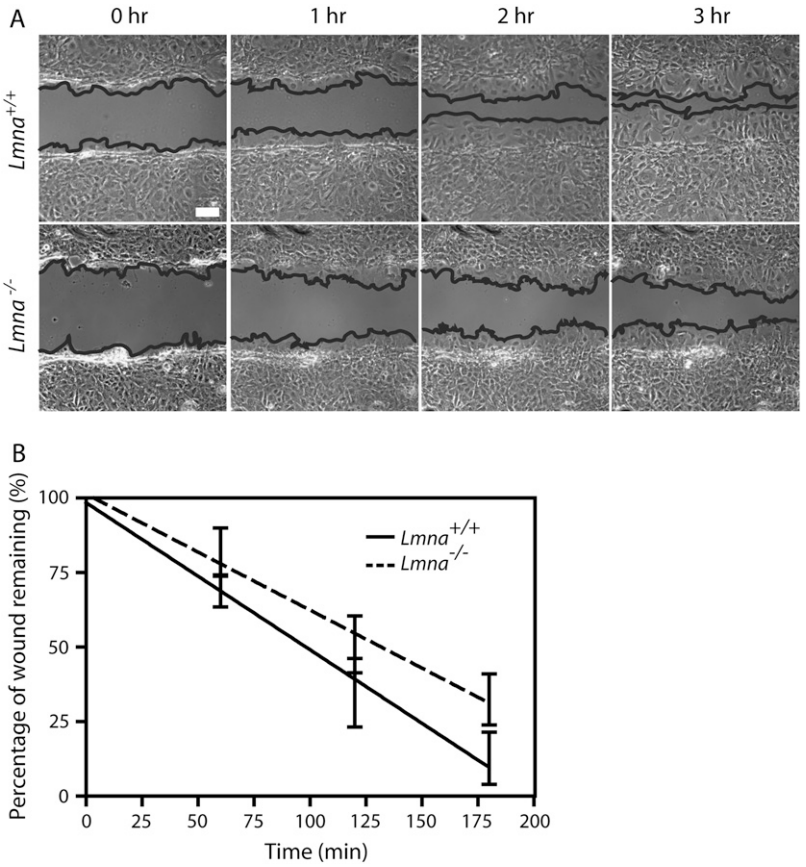

FIGURE 4 Diminished speed of migration of MEFs lacking lamin A/C during wound healing. (*A*) Phase contrast micrographs of $Lmna^{+/+}$ MEFs (*top*) and $Lmna^{-/-}$ MEFs (*bottom*) immediately after wounding, and 1, 2, and 3 h after wounding. The edges of the wounds are traced as guides to the eye. Bar, 100 μm. (*B*) Fraction of the wound that remains uncovered by the crawling cells as a function of time for $Lmna^{+/+}$ MEFs (*bottom*) and $Lmna^{-/-}$ MEFs (*top*) ($n = 7$ for each type of cell).

linked to the rubber bands and forces are locally applied on one side of the bag, then the ball moves easily toward the other side of the bag and the apparent global stiffness of the toy is low. However, if the rubber bands are now physically linked to the ball, then the interconnected ball cannot be moved around easily, which allows the ball to contribute, and enhance, the global stiffness of the toy. Previous composite measurements are unable to ascertain whether this link exists, and can only measure apparent changes in global cell stiffness (see more below). Showing that lamin A/C deficiency does not significantly affect the mechanical properties of the perinuclear region indicates that the nucleus (i.e., the ball in the toy model) did not appreciably change in stiffness, but that the link between nucleus and cytoskeleton was

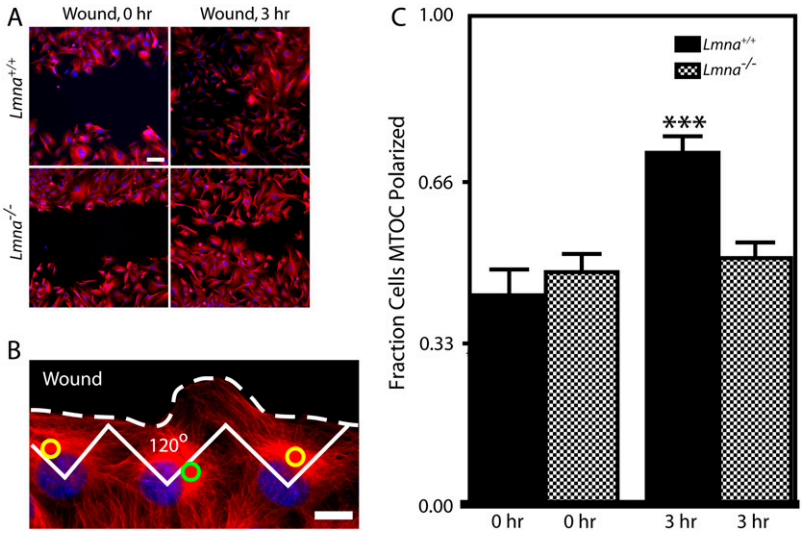

FIGURE 5 Impaired MTOC repositioning in MEFs lacking lamin A/C. (*A*) $Lmna^{+/+}$ MEFs and $Lmna^{-/-}$ MEFs immediately after a wound and 3 h after the wound. Cells were fixed and microtubule and nuclear DNA were stained using α-tubulin/Alexa568 and DAPI, respectively. Bar, 100 μm. (*B*) Microtubule network organization in $Lmna^{+/+}$ MEFs at the edge of the wound. Cells at the edge of the wound, which have their MTOC preferentially located within the front third facing the wound, are considered polarized (*yellow circles*); cells that have their MTOC located in the back two-thirds of the cell are considered nonpolarized (*green circle*). Bar, 20 μm. (*C*) Fractions of $Lmna^{+/+}$ MEFs and $Lmna^{-/-}$ MEFs that had a polarized MTOC before the wound (0 h) and 3 h after wounding. For $Lmna^{+/+}$ MEFs, $n = 91$ cells at 0 h and $n = 175$ cells at 3 h. For $Lmna^{-/-}$ MEFs, $n = 183$ cells at 0 h and $n = 242$ cells at 3 h.

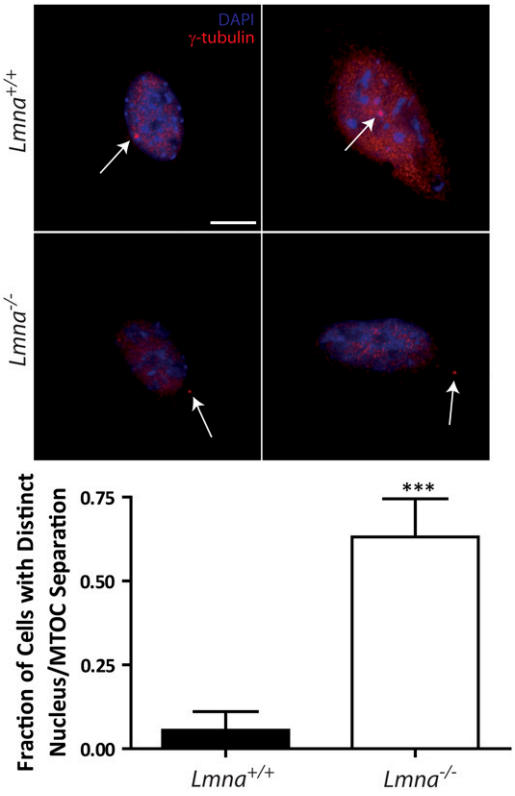

FIGURE 6 Separation between MTOC and nucleus induced by lamin A/C deficiency. (*Top*) Immnufluorescence micrographs of $Lmna^{+/+}$ MEFs and $Lmna^{-/-}$ MEFs showing the position of the MTOC marked by γ-tubulin (*thin arrows*) stained using γ-tubulin/Alexa568 and the nucleus delineated by DAPI staining of nuclear DNA. Top row, typical $Lmna^{+/+}$ MEFs; bottom row, typical $Lmna^{-/-}$ MEFs. Bar, 20 μm. (*Bottom*) Fraction of cells with a distinct separation between MTOC and nucleus. A value of 0 was assigned to a cell if the MTOC touched or laid on top or bottom of the nucleus, whereas a value of 1 was assigned to a cell if the MTOC was clearly separated from the nucleus. At least 20 cells were assayed for each type of cell.

either ruptured or significantly weakened. Indeed, when cytoskeleton and nucleus are disconnected through lamin A/C deficiency, the cytoplasm softens to levels down to those observed when actin or microtubule networks are disassembled. These results also suggest that the molecular links between the cytoskeleton and the nucleus—LINC complex to the actin network (29) and hook-like proteins to the microtubule network (44)—are functional, profoundly affecting important cytoskeleton-based cell functions, including cell motility and polarization.

Our observed changes in cytoplasmic stiffness caused by lamin A/C deficiency could stem not from a weakening of the physical connection between the nucleus and the cytoskeleton, but from changes in the levels of expression of cytoskeleton proteins caused by the elimination of the *Lmna* gene. However, an array analysis comparing gene expression in $Lmna^{+/+}$ MEFs and $Lmna^{-/-}$ MEFs shows relatively few differences. Approximately 40 genes were either up- or downregulated out of 35,000. None of these genes were cytoskeletal proteins or were known to have any direct effects on the cytoskeleton or cytoskeletal structures (D. Cutler and C. L. Stewart, unpublished observations).

In this study, our choice of BIN to measure cell mechanics allowed us to circumvent the drawbacks associated with previously described methods applied to the same cells and to extract local information regarding cellular mechanics. Indeed, Lammerding et al. used the magnetic bead twisting method to probe the influence of lamin A/C deficiency on cell mechanics (26). In this approach, large fibronectin (FN)-coated magnetic beads are tethered to the outer face of the plasma membrane and subjected to magnetic forces; the global mechanical response of the cell is measured in terms of the extent of rotation of the beads (49). This approach probes the composite mechanical response of different organelles, including the cytoskeleton in the body of the cell, the plasma and nuclear membranes, the nucleoskeleton, and the actin cytoskeleton bound to the inner face of the plasma membrane and artificially recruited toward the bead through integrin activation and clustering by fibronectin on the bead. Therefore, the magnetic bead twisting method cannot readily disentangle the contribution of the cytoskeleton from the contributions of the plasma membrane and the nucleus to cell mechanics. Efforts were made to probe beads away from the nucleus (26), but it is well established that the imposed displacements of a FN-coated bead tethered to the plasma membrane results in large deformations over the entire cell that mechanically engage the nucleus (49,50). Moreover, the surface area of contact between the bead and the cell surface is not controlled and apparent changes in MEF mechanics may be caused by different extents of engulfment of the bead into the cell membrane, not directly by changes in the mechanical properties of the cytoplasm.

In contrast, BIN measures directly the local viscoelastic properties of the cytoplasm using small nanoscale probes located inside the cell and subjected to minuscule Brownian random forces. BIN measures the absolute values of the rheological parameters that characterize the full mechanical response of the cytoskeleton—including mechanical compliance, viscosity, and elasticity—which can then be compared to those measured in other cell types or to those obtained with reconstituted cytoskeleton networks or predicted by computational models of cell and nucleus mechanics (51). Furthermore, BIN measures the rate dependence of the mechanical response of the cytoplasm, i.e., the values of the viscosity and elasticity of the cytoplasm when it is sheared slowly or rapidly. Also, the known viscosity and elasticity of standard liquids and materials measured by particle tracking nanorheology compared favorably with those measured by conventional bulk rheometers (52–54). Therefore, the presence of the nanoparticles does not affect the measurement of materials properties. The membrane-tethering requirement of the magnetic twisting method prevents this method from being easily tested on standard fluids of known viscoelasticity.

Finally, BIN probes the local properties of the cytoplasm: BIN can distinguish and compare the mechanical properties of the cytoskeleton in the vicinity of the nucleus to those of the cytoskeleton in the cell periphery. Therefore, unlike previous approaches, BIN allows us to measure rigorously the local mechanics of the cytoplasm in $Lmna^{-/-}$ and $Lmna^{+/+}$ MEFs and test directly the hypothesis that the absence of lamin A/C affects the rheology of the cytoskeleton.

Immunofluorescence microscopy did not reveal obvious differences in the cytoskeletal architectures of MEFs caused by lamin A/C deficiency. This may be in part due to the limited resolution of immunofluorescence microscopy, which cannot show subtle changes in actin organization (55). Moreover, slight changes in local protein concentrations (such as cross-linking proteins (32)), which do not lead to dramatic changes in cytoskeleton organization, may create large changes in cytoskeleton stiffness. For instance, serum-starved fibroblasts stimulated by lysophospatidic acid (LPA) and shear flows display similar actin organizations. Yet, shear flows induce a 10-fold more pronounced stiffening of the cytoskeleton than LPA (30,38). This underlines the importance of a functional assay, such as BIN, when probing cytoskeleton function.

Impaired cell migration and polarization induced by lamin A/C deficiency

Our previous work shows that fibroblasts stiffen their cytoplasm to migrate into a wound (34). Indeed, net propulsive forces stemming from actin assembly occur only when the pointed ends of the filaments are able to push against a stiff cytoplasm (51,56). Therefore, we hypothesized that our observed softening of the cytoplasm in cells lacking nuclear lamin A/C would affect their speed of migration. We find that the absence of nuclear lamin A/C significantly reduces actin-assembly powered motility of $Lmna^{-/-}$ MEFs. Together these results indicate that lamin A/C deficiency softens greatly the cytoskeleton, which in turn reduces significantly the speed of migration of $Lmna^{-/-}$ MEFs into a wound. Once again, these results suggest the existence of a functional connection between actin cytoskeleton and nucleus, which plays a key role in cell motility.

We find that nuclear lamin A/C deficiency largely abrogates the ability of fibroblasts to polarize their microtubule cytoskeleton toward the wound. Migrating cells at the edge of a wounded monolayer exhibit a polarized microtubule structure where the MTOC preferentially faces the direction of migration (39,40). In fibroblasts, such changes are controlled by the small GTPase Cdc42 via downstream effectors Par6 and PKCζ, not the small GTPases Rho and Rac (42). The Cdc42/Par6/PKCζ complex mediates signaling pathways that causes downstream MT reorganization (41,57,58) and subsequent repositioning of the MTOC in the direction of the wound. Such repositioning has been shown to result in nucleus rotation and movement, possibly through direct interactions between the MTOC and the nucleus (42). Since we found that lamin A/C deficiency creates significant separation between MTOC and nucleus, our results also suggest that cell polarization during cell migration requires tight mechanical coupling between the MTOC and the nucleus, which is mediated by lamin A/C. Nucleus-cytoskeleton interactions may involve homologs of Hook proteins, as recent work has shown that in *C. elegans*, ZYG-12, a member of the Hook family of cytoskeletal link proteins, couples the MTOC to the nucleus via SUN proteins during embryogenesis (44). Our previous results suggest a similar mechanism exists in mammalian cells to regulate nucleus movement and rotation observed in sheared cells (42). Together these results suggest that the lack of polarization in $Lmna^{-/-}$ MEFs is due to the rupture of the MTOC-nucleus link mediated by the absence of lamin A/C in the nucleus.

Implications for lamin-based diseases

Our results suggest that, in addition to the reported ultrastructural anomalies of the nuclear envelope in many laminopathic tissues and model cell cultures, the structural anomalies resulting from the lack or mutation of lamin A/C extends far beyond the nuclear envelope to affect the whole cytoskeleton organization and cytoskeleton-based cell functions. The actin and microtubule networks are certainly affected. In addition, intermediate filaments networks might also be affected since a disorganization of the desmin network has been shown in cardiomyocytes lacking lamin A/C (28) and in cardiac muscle of $Lmna^{N195K/N195K}$ animals (20). These observations further reinforce the existence of additional molecular connections linking the nuclear lamina to the cytoskeleton that remain to be discovered.

The authors thank the reviewers for helpful suggestions.

This work was supported by a National Institutes of Health grant (R01 GM075305-01) and a Howard Hughes Medical Institute graduate training grant, both to D.W. J.S.H.L. and T.P. were supported by National Aeronautics and Space Administration graduate fellowships. D.H. was supported by the Muscular Dystrophy Association.

REFERENCES

1. Hetzer, M. W., T. C. Walther, and I. W. Mattaj. 2005. Pushing the envelope: structure, function, and dynamics of the nuclear periphery. *Annu. Rev. Cell Dev. Biol.* 21:347–380.
2. Hutchison, C. J. 2002. Lamins: building blocks or regulators of gene expression? *Nat. Rev. Mol. Cell Biol.* 3:848–858.
3. Stuurman, N., S. Heins, and U. Aebi. 1998. Nuclear lamins: their structure, assembly, and interactions. *J. Struct. Biol.* 122:42–66.
4. Elbashir, S. M., J. Harborth, W. Lendeckel, A. Yalcin, K. Weber, and T. Tuschl. 2001. Duplexes of 21-nucleotide RNAs mediate RNA interference in cultured mammalian cells. *Nature.* 411:494–498.
5. Vergnes, L., M. Peterfy, M. O. Bergo, S. G. Young, and K. Reue. 2004. Lamin B1 is required for mouse development and nuclear integrity. *Proc. Natl. Acad. Sci. USA.* 101:10428–10433.

6. Burke, B., and C. L. Stewart. 2002. Life at the edge: the nuclear envelope and human disease. *Nat. Rev. Mol. Cell Biol.* 3:575–585.
7. Gruenbaum, Y., A. Margalit, R. D. Goldman, D. K. Shumaker, and K. L. Wilson. 2005. The nuclear lamina comes of age. *Nat. Rev. Mol. Cell Biol.* 6:21–31.
8. Bonne, G., M. R. Di Barletta, S. Varnous, H. M. Becane, E. H. Hammouda, L. Merlini, F. Muntoni, C. R. Greenberg, F. Gary, J. A. Urtizberea, D. Duboc, M. Fardeau, et al. 1999. Mutations in the gene encoding lamin A/C cause autosomal dominant Emery-Dreifuss muscular dystrophy. *Nat. Genet.* 21:285–288.
9. Fatkin, D., C. MacRae, T. Sasaki, M. R. Wolff, M. Porcu, M. Frenneaux, J. Atherton, H. J. Vidaillet Jr., S. Spudich, U. De Girolami, J. G. Seidman, C. Seidman, et al. 1999. Missense mutations in the rod domain of the lamin A/C gene as causes of dilated cardiomyopathy and conduction-system disease. *N. Engl. J. Med.* 341:1715–1724.
10. Cao, H., and R. A. Hegele. 2000. Nuclear lamin A/C R482Q mutation in Canadian kindreds with Dunnigan-type familial partial lipodystrophy. *Hum. Mol. Genet.* 9:109–112.
11. Muchir, A., B. G. van Engelen, M. Lammens, J. M. Mislow, E. McNally, K. Schwartz, and G. Bonne. 2003. Nuclear envelope alterations in fibroblasts from LGMD1B patients carrying nonsense Y259X heterozygous or homozygous mutation in lamin A/C gene. *Exp. Cell Res.* 291:352–362.
12. De Sandre-Giovannoli, A., M. Chaouch, S. Kozlov, J. M. Vallat, M. Tazir, N. Kassouri, P. Szepetowski, T. Hammadouche, A. Vandenberghe, C. L. Stewart, D. Grid, and N. Levy. 2002. Homozygous defects in LMNA, encoding lamin A/C nuclear-envelope proteins, cause autosomal recessive axonal neuropathy in human (Charcot-Marie-Tooth disorder type 2) and mouse. *Am. J. Hum. Genet.* 70:726–736.
13. Novelli, G., A. Muchir, F. Sangiuolo, A. Helbling-Leclerc, M. R. D'Apice, C. Massart, F. Capon, P. Sbraccia, M. Federici, R. Lauro, C. Tudisco, R. Pallotta, et al. 2002. Mandibuloacral dysplasia is caused by a mutation in LMNA-encoding lamin A/C. *Am. J. Hum. Genet.* 71:426–431.
14. Mounkes, L., S. Kozlov, B. Burke, and C. L. Stewart. 2003. The laminopathies: nuclear structure meets disease. *Curr. Opin. Genet. Dev.* 13:223–230.
15. Eriksson, M., W. T. Brown, L. B. Gordon, M. W. Glynn, J. Singer, L. Scott, M. R. Erdos, C. M. Robbins, T. Y. Moses, P. Berglund, A. Dutra, E. Pak, et al. 2003. Recurrent de novo point mutations in lamin A cause Hutchinson-Gilford progeria syndrome. *Nature.* 423:293–298.
16. Csoka, A. B., H. Cao, P. J. Sammak, D. Constantinescu, G. P. Schatten, and R. A. Hegele. 2004. Novel lamin A/C gene (LMNA) mutations in atypical progeroid syndromes. *J. Med. Genet.* 41:304–308.
17. Ben Yaou, R., A. Muchir, T. Arimura, C. Massart, L. Demay, P. Richard, and G. Bonne. 2005. Genetics of laminopathies. *Novartis Found. Symp.* 264:81–90; discussion 90–97, 227–230.
18. Sullivan, T., D. Escalante-Alcalde, H. Bhatt, M. Anver, N. Bhat, K. Nagashima, C. L. Stewart, and B. Burke. 1999. Loss of A-type lamin expression compromises nuclear envelope integrity leading to muscular dystrophy. *J. Cell Biol.* 147:913–920.
19. Mounkes, L. C., S. Kozlov, L. Hernandez, T. Sullivan, and C. L. Stewart. 2003. A progeroid syndrome in mice is caused by defects in A-type lamins. *Nature.* 423:298–301.
20. Mounkes, L. C., S. V. Kozlov, J. N. Rottman, and C. L. Stewart. 2005. Expression of an LMNA-N195K variant of A-type lamins results in cardiac conduction defects and death in mice. *Hum. Mol. Genet.* 14:2167–2180.
21. Arimura, T., A. Helbling-Leclerc, C. Massart, S. Varnous, F. Niel, E. Lacene, Y. Fromes, M. Toussaint, A. M. Mura, D. I. Keller, H. Amthor, et al. 2005. Mouse model carrying H222P-Lmna mutation develops muscular dystrophy and dilated cardiomyopathy similar to human striated muscle laminopathies. *Hum. Mol. Genet.* 14:155–169.
22. Zastrow, M. S., S. Vlcek, and K. L. Wilson. 2004. Proteins that bind A-type lamins: integrating isolated clues. *J. Cell Sci.* 117:979–987.
23. Goldman, R. D., A. E. Goldman, and D. K. Shumaker. 2005. Nuclear lamins: building blocks of nuclear structure and function. *Novartis Found. Symp.* 264:3–16; discussion 16–21, 227–230.
24. Bridger, J. M., and I. R. Kill. 2004. Aging of Hutchinson-Gilford progeria syndrome fibroblasts is characterised by hyperproliferation and increased apoptosis. *Exp. Gerontol.* 39:717–724.
25. Broers, J. L., E. A. Peeters, H. J. Kuijpers, J. Endert, C. V. Bouten, C. W. Oomens, F. P. Baaijens, and F. C. Ramaekers. 2004. Decreased mechanical stiffness in LMNA−/− cells is caused by defective nucleocytoskeletal integrity: implications for the development of laminopathies. *Hum. Mol. Genet.* 13:2567–2580.
26. Lammerding, J., P. C. Schulze, T. Takahashi, S. Kozlov, T. Sullivan, R. D. Kamm, C. L. Stewart, and R. T. Lee. 2004. Lamin A/C deficiency causes defective nuclear mechanics and mechanotransduction. *J. Clin. Invest.* 113:370–378.
27. Maniotis, A. J., C. S. Chen, and D. E. Ingber. 1997. Demonstration of mechanical connections between integrins, cytoskeletal filaments, and nucleoplasm that stabilize nuclear structure. *Proc. Natl. Acad. Sci. USA.* 94:849–854.
28. Nikolova, V., C. Leimena, A. C. McMahon, J. C. Tan, S. Chandar, D. Jogia, S. H. Kesteven, J. Michalicek, R. Otway, F. Verheyen, S. Rainer, C. L. Stewart, et al. 2004. Defects in nuclear structure and function promote dilated cardiomyopathy in lamin A/C-deficient mice. *J. Clin. Invest.* 113:357–369.
29. Crisp, M., Q. Liu, K. Roux, J. B. Rattner, C. Shanahan, B. Burke, P. D. Stahl, and D. Hodzic. 2006. Coupling of the nucleus and cytoplasm: role of the LINC complex. *J. Cell Biol.* 172:41–53.
30. Lee, J. S., P. Panorchan, C. M. Hale, S. B. Khatau, T. P. Kole, Y. Tseng, and D. Wirtz. 2006. Ballistic intracellular nanorheology reveals ROCK-hard cytoplasmic stiffening response to fluid flow. *J. Cell Sci.* 119:1760–1768.
31. Panorchan, P., J. S. Lee, T. P. Kole, Y. Tseng, and D. Wirtz. 2006. Microrheology and ROCK signaling of human endothelial cells embedded in a 3D matrix. *Biophys. J.* 91:3499–3507.
32. Tseng, Y., T. P. Kole, and D. Wirtz. 2002. Micromechanical mapping of live cells by multiple-particle-tracking microrheology. *Biophys. J.* 83: 3162–3176.
33. Kole, T. P., Y. Tseng, and D. Wirtz. 2004. Intracellular microrheology as a tool for the measurement of the local mechanical properties of live cells. *Methods Cell Biol.* 78:45–64.
34. Kole, T. P., Y. Tseng, I. Jiang, J. L. Katz, and D. Wirtz. 2005. Intracellular mechanics of migrating fibroblasts. *Mol. Biol. Cell.* 16:328–338.
35. Haber, C., S. A. Ruiz, and D. Wirtz. 2000. Shape anisotropy of a single random-walk polymer. *Proc. Natl. Acad. Sci. USA.* 97:10792–10795.
36. Xu, J. Y., V. Viasnoff, and D. Wirtz. 1998. Compliance of actin filament networks measured by particle-tracking microrheology and diffusing wave spectroscopy. *Rheol. Acta.* 37:387–398.
37. Tseng, Y., K. M. An, O. Esue, and D. Wirtz. 2004. The bimodal role of filamin in controlling the architecture and mechanics of F-actin networks. *J. Biol. Chem.* 279:1819–1826.
38. Kole, T. P., Y. Tseng, L. Huang, J. L. Katz, and D. Wirtz. 2004. Rho kinase regulates the intracellular micromechanical response of adherent cells to rho activation. *Mol. Biol. Cell.* 15:3475–3484.
39. Palazzo, A. F., H. L. Joseph, Y. J. Chen, D. L. Dujardin, A. S. Alberts, K. K. Pfister, R. B. Vallee, and G. G. Gundersen. 2001. Cdc42, dynein, and dynactin regulate MTOC reorientation independent of Rho-regulated microtubule stabilization. *Curr. Biol.* 11:1536–1541.
40. Etienne-Manneville, S., and A. Hall. 2003. Cdc42 regulates GSK-3beta and adenomatous polyposis coli to control cell polarity. *Nature.* 421:753–756.
41. Etienne-Manneville, S., and A. Hall. 2001. Integrin-mediated activation of Cdc42 controls cell polarity in migrating astrocytes through PKCzeta. *Cell.* 106:489–498.
42. Lee, J. S., M. I. Chang, Y. Tseng, and D. Wirtz. 2005. Cdc42 mediates nucleus movement and MTOC polarization in Swiss 3T3 fibroblasts under mechanical shear stress. *Mol. Biol. Cell.* 16:871–880.
43. Zhen, Y. Y., T. Libotte, M. Munck, A. A. Noegel, and E. Korenbaum. 2002. NUANCE, a giant protein connecting the nucleus and actin cytoskeleton. *J. Cell Sci.* 115:3207–3222.

44. Malone, C. J., L. Misner, N. Le Bot, M. C. Tsai, J. M. Campbell, J. Ahringer, and J. G. White. 2003. The C. elegans hook protein, ZYG-12, mediates the essential attachment between the centrosome and nucleus. *Cell*. 115:825–836.

45. Lee, K. K., D. Starr, M. Cohen, J. Liu, M. Han, K. L. Wilson, and Y. Gruenbaum. 2002. Lamin-dependent localization of UNC-84, a protein required for nuclear migration in Caenorhabditis elegans. *Mol. Biol. Cell*. 13:892–901.

46. Malone, C. J., W. D. Fixsen, H. R. Horvitz, and M. Han. 1999. UNC-84 localizes to the nuclear envelope and is required for nuclear migration and anchoring during C. elegans development. *Development*. 126:3171–3181.

47. Starr, D. A., and M. Han. 2002. Role of ANC-1 in tethering nuclei to the actin cytoskeleton. *Science*. 298:406–409.

48. Starr, D. A., and M. Han. 2003. ANChors away: an actin based mechanism of nuclear positioning. *J. Cell Sci*. 116:211–216.

49. Wang, N., and D. E. Ingber. 1995. Probing transmembrane mechanical coupling and cytomechanics using magnetic twisting cytometry. *Biochem. Cell Biol*. 73:327–335.

50. Bausch, A. R., W. Moller, and E. Sackmann. 1999. Measurement of local viscoelasticity and forces in living cells by magnetic tweezers. *Biophys. J*. 76:573–579.

51. Atilgan, E., D. Wirtz, and S. X. Sun. 2005. Morphology of the lamellipodium and organization of actin filaments at the leading edge of crawling cells. *Biophys. J*. 89:3589–3602.

52. Mason, T. G., K. Ganesan, J. H. vanZanten, D. Wirtz, and S. C. Kuo. 1997. Particle tracking microrheology of complex fluids. *Phys. Rev. Lett*. 79:3282–3285.

53. Palmer, A., J. Xu, S. C. Kuo, and D. Wirtz. 1999. Diffusing wave spectroscopy microrheology of actin filament networks. *Biophys. J*. 76:1063–1071.

54. Apgar, J., Y. Tseng, E. Federov, M. B. Herwig, S. C. Almo, and D. Wirtz. 2000. Multiple-particle tracking measurements of heterogeneities in solutions of actin filaments and actin bundles. *Biophys. J*. 79:1095–1106.

55. Svitkina, T. M., and G. G. Borisy. 1998. Correlative light and electron microscopy of the cytoskeleton of cultured cells. *Methods Enzymol*. 298:570–592.

56. Atilgan, E., D. Wirtz, and S. X. Sun. 2006. Mechanics and dynamics of actin-driven thin membrane protrusions. *Biophys. J*. 90:65–76.

57. Tzima, E., W. B. Kiosses, M. A. del Pozo, and M. A. Schwartz. 2003. Localized cdc42 activation, detected using a novel assay, mediates microtubule organizing center positioning in endothelial cells in response to fluid shear stress. *J. Biol. Chem*. 278:31020–31023.

58. Joberty, G., C. Petersen, L. Gao, and I. G. Macara. 2000. The cell-polarity protein Par6 links Par3 and atypical protein kinase C to Cdc42. *Nat. Cell Biol*. 2:531–539.